Journal of Materials Chemistry C

ROYAL SOCIETY OF CHEMISTRY

PAPER

View Article Online
View Journal | View Issue

Cite this: J. Mater. Chem. C, 2025, 13, 20549

Saturated carbazole-embedded BN-aromatic systems as narrowband sky-blue emitters

Mahni Fatahi, Aidan P. McKay, David B. Cordes and Eli Zysman-Colman *

Due to their rigid structure and short-range charge transfer emissive excited states, multiresonant thermally activated delayed fluorescence (MR-TADF) emitters provide exceptional color purity due to their narrowband emission. Many examples are based on nitrogen/boron-doped polycyclic aromatic hydrocarbons. The emission color is in part modulated by the strength of the donor heterocycle. In an effort to shift the emission to the blue, we explore in this study the partial saturation of the carbazole donor. We designed four emitters-**tButHCzB**, **DtButHCzB**, **SpAc-tButHCzB**, and **SpAc-DtButHCzB** featuring tetrahydrocarbazole donor moieties, which disrupt the planarity and reduce the conjugation length. Theoretical calculations predict moderate singlet–triplet excited-state energy gaps (ΔE_{ST} = 250–270 meV) and low-lying T_2 and T_3 states, suggesting that these compounds should exhibit TADF. In toluene, the four compounds emit in the sky-blue region (λ_{PL} = 476–480 nm), with narrow full-width at half-maximum (FWHM) values (18–21 nm) and high photoluminescence quantum yields (Φ_{PL}) of 86–91%. In 1 wt% doped films in mCP, however, their Φ_{PL} drops to between 40–45% and their emission slightly red-shifts to λ_{PL} of 483–491 nm. Temperature-dependent time-resolved PL measurements confirm that these compounds exhibit TADF. This study offers valuable insights into a region of chemical space scantly explored in MR-TADF emitter design.

Received 30th June 2025,
Accepted 26th August 2025

DOI: 10.1039/d5tc02496j

rsc.li/materials-c

Introduction

Thermally activated delayed fluorescence (TADF) emitters have emerged recently as an alternative and promising class of materials to phosphorescence complexes for use in organic light-emitting diodes (OLEDs).[1] This is largely due to their comparable exciton utilization efficiency in electroluminescent devices to phosphorescent materials. A subclass of TADF emitters, so-called multiresonant TADF (MR-TADF) compounds, provide desirable narrowband emission required for high-definition displays, due to their rigid structure typically based on a p- and n-doped polycyclic aromatic hydrocarbon skeleton. The regiochemistry of the p- and n-dopants produces an excited state of short-range charge-transfer (SRCT) character that results in a moderately small singlet–triplet excited-state energy gap, ΔE_{ST}, on the order of 200 meV.[1–4] In particular, to meet the blue BT.2020 industry standard, narrowband emission is important both to reduce the amount of UV-light that is being emitted and to decrease the excitation energy that results in greater photochemical stability of the emitter material.[5,6]

OLEDs are typically fabricated by vacuum deposition. An alternative fabrication methodology is to use solution-processing technologies, which offer the promise of more cost-effective and less material-wasteful manufacture of the device.[7–10] This requires the use of a solution-processable emitter, which necessitates that this material be suitably soluble in the organic solvents used to process it into a film and that the resulting film be homogeneous.[1,11] A primary strategy to achieve greater solubilities in these rigid, planar molecules, is to disrupt their planarity through the introduction of bulky substituents and/or to increase the conformational flexibility by saturating the rings within the core structure, the latter strategy of which has not been extensively explored. We previously documented that the incorporation of mesityl groups in **Mes$_3$-DiKTa**[12] increases the solubility of this compound in chlorobenzene (**Mes$_3$-DiKTa:** 20 mg mL^{-1}; **DiKTa:** 12.5 mg mL^{-1}) and mitigates aggregation-caused quenching (ACQ) in spin-coated films and in the vacuum-deposited device. This substitution also causes a red-shift in the emission from λ_{PL} of 453 nm for the parent compound **DiKTa** (aka **QAO**[13]) to 468 nm for **Mes$_3$-DiKTa** in dilute toluene solution. This is due to the inductively electron-withdrawing nature of the mesityl substituents. Wu *et al.* likewise demonstrated how decorating the **DABNA-1**[14] core with methyl, mesityl, and adamantyl substituents in **A-BN**, **DA-BN**, and **A-DBN**[15] reduces ACQ, and maintains the blue emission in **A-BN** with a λ_{PL} of 462 nm. Yet additional substitutions to prevent quenching even further lead to a red-shifted emission

Organic Semiconductor Centre, EaStCHEM School of Chemistry, University of St Andrews, St Andrews, UK KY16 9ST. E-mail: eli.zysman-colman@st-andrews.ac.uk

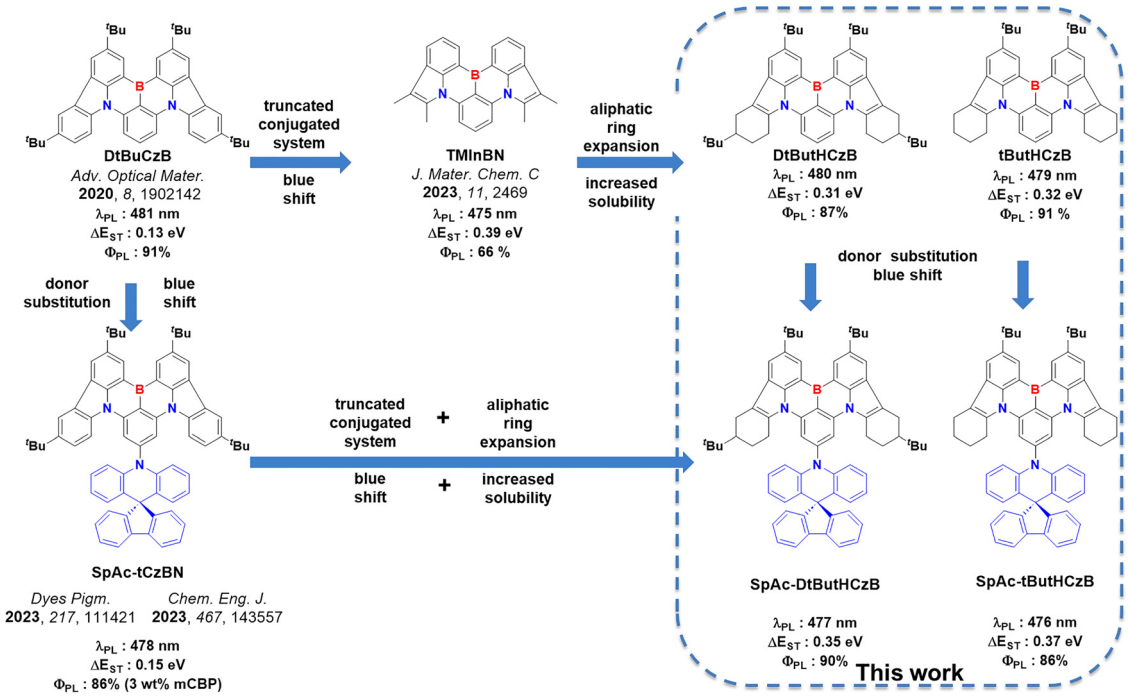

Fig. 1 Chemical structures of relevant emitters in the literature[16,18–20] and the four novel emitters **DtButHCzB**, **tButHCzB**, **SpAc-DtButHCzB** and **SpAc-tButHCzB** introduced in this study.

from λ_{PL} of 462 nm for **DABNA-1** to 483 nm for **DA-BN** and 482 nm for **A-DBN** in dilute dichloromethane solution.

A different approach was taken by Du *et al.* for **TImBN**[16] (Fig. 1) in which they truncated the carbazole units of **CzBN**[17] and incorporated instead 2,3-dimethyl-1*H*-indole moieties. By truncating the aromatic system and effectively decreasing the conjugation length, this compound shows a slightly blue-shifted emission peaking at λ_{PL} of 475 nm compared to **DtBuCzB**[18] (λ_{PL} = 481 nm) in dilute toluene solution. However, **TImBN** possesses a significantly larger ΔE_{ST} of 390 meV compared to **DtBuCzB** (ΔE_{ST} = 130 meV),[18] which makes the thermally promoted exciton upconversion kinetics much less favourable. The authors also demonstrated that a blue-shift in the emission to λ_{PL} of 470 nm in dilute toluene could be induced by attaching a 3,6-di-*tert*-butylcarbazole donor moiety *para* to the boron atom on the central ring. However, the T_1 level remains unaffected by this substitution, leading to an even larger ΔE_{ST} of 420 meV, which means that this compound is unlikely to emit by TADF, despite the authors' claims to the contrary.

Here, we investigate an approach to introduce saturation into one of the rings of the carbazole moieties of the parent **DtBuCzB** emitter in order to blue-shift the emission and increase the solubility to make these derivatives compatible for solution-processed OLEDs (SP-OLEDs). We designed and synthesized four emitters, **tButHCzB**, **DtButHCzB**, **SpAc-tButHCzB**, and **SpAc-DtButHCzB**, where we replaced the 3,6-di-*tert*-butyl carbazole with either 6-(*tert*-butyl)-2,3,4,9-tetrahydrocarbazole (**tButHCz**) or 3,6-di-*tert*-butyl-2,3,4,9-tetrahydrocarbazole (**DtButHCz**) donor moieties (Fig. 1). By saturating one of the phenyl rings of the carbazole, this moiety becomes less planar, and the size of the conjugated system decreases, hence promoting an expected and desired blue-shift of the emission. Two derivatives of these two compounds, **SpAc-tButHCzB** and **SpAc-DtButHCzB**, also contain a spiro[acridine-9,9′-fluorene] donor moiety positioned *para* to the boron atom on the central benzene ring to promote a further blue-shift of the emission. Theoretical calculations at the RI-wPBEPP866/cc-pVDZ level of theory predict moderate ΔE_{ST} of 250–270 meV and close-lying T_2 and T_3 states that suggest that these four compounds should be TADF. In dilute toluene solution, the four emitters show sky-blue photoluminescence (PL) at λ_{PL} of 476–480 nm and very narrowband emission with full-width half maxima (FWHM) of 18–21 nm. All four emitters have high photoluminescence quantum yields, Φ_{PL}, of 86–91%, though no delayed emission was detected in solution. The photophysics of the spin-coated 1 wt% doped films in 1,3-bis(*N*-carbazolyl)benzene (mCP) revealed an undesired red-shifting and broadening of the emission band (λ_{PL} of 483–491 nm and FWHM of 26–45 nm), ascribed to the formation of π-stacked aggregates, even at this low doping concentration, that are also present in the single crystal X-ray structures. This is accompanied by a noted significant decrease in the Φ_{PL} to 40–45%, thus decreasing their value as emitters for OLEDs. This study reveals for the first time, structure–property relationships in MR-TADF emitters containing partially saturated N-heterocyclic donor moieties.

Results and discussion

Synthesis and characterisation

The synthesis of **tButHCzB** and **DtButHCzB** was carried out in three steps as shown in Scheme 1, and for **SpAc-tButHCzB** and

SpAc-DtButHCzB in four steps. The first step for all four emitters was a Fisher-indole synthesis using (4-(*tert*-butyl)-phenyl)hydrazine hydrochloride and 4-(*tert*-butyl)cyclohexan-1-one or cyclohexan-1-one to construct the tetrahydrocarbazole derivative **1** or **2** in yields of 74 and 90%, respectively. For **tButHCzB** and **DtButHCzB**, an S_NAr reaction between 2-bromo-1,3-difluorobenzene and two equivalents of the respective tetrahydrocarbazole gave intermediates **3** and **4** in 45 and 20% yields, respectively. Spiro-acridine-containing derivatives **SpAc-tButHCzB** and **SpAc-DtButHCzB** were obtained by first reacting **1** and **2** with 5-bromo-2-chloro-1,3-difluorobenzene under S_NAr conditions to give intermediates **5** and **6** in 77 and 71% yields, respectively, followed by a Buchwald–Hartwig coupling with 10*H*-spiro[acridine-9,9′-fluorene] to afford **7** and **8** in 89 and 71% yields, respectively. The final step for all four emitters consisted of a one-pot borylation using *tert*-butyl lithium, boron tribromide and diisopropylethylamine[14] to afford the target emitters **tButHCzB**, **DtButHCzB**, **SpAc-tButHCzB** and **SpAc-DtButHCzB** in 13, 22, 29, and 39%, respectively. Their structure and purity were verified using a combination of ^{1}H NMR and ^{13}C NMR spectroscopy, high-resolution mass spectrometry, elemental analysis, single-crystal XRD, and melting point determination. Emitters containing only two *tert*-butyl groups have significantly lower melting points (**tButHCzB** and **SpAc-tButHCzB** showed melting points of 315–318 and 330–334 °C, respectively) than their analogues with four *tert*-butyl groups (**DtButHCzB** and **SpAc-DtButHCzB** showed melting points of 357–361 and >400 °C, respectively). This is not only due to the increased molecular weight but also that the second *tert*-butyl group locks the conformation of the cyclohexenyl ring. In thermogravimetric analysis a different trend is observed, here **tButHCzB** has the lowest degradation temperature, T_d at 5% weight loss (354 °C) followed by **DtButHCzB** (375 °C). Surprisingly **tButHCzB** shows the highest T_d of 497 °C (Fig. S9).

X-ray crystal structures

Crystals of three emitters, **tButHCzB**, **SpAc-DtButHCzB**, and **SpAc-tButHCzB**, suitable for single crystal diffraction were grown by a slow diffusion of antisolvent (methanol or isopropanol) into a saturated solution of the emitter in either dichloromethane or toluene (SI for details). Crystals of **DtButHCzB** were also obtained but were poorly diffracting and gave unsatisfactory data. A solution from this data did show connectivity consistent with the expected structure (Fig. S1). The structures obtained are consistent with the proposed molecular structures (Fig. 2 and Fig. S2–S4), with **SpAc-tButHCzB**, and **SpAc-DtButHCzB** crystallising as toluene and hexane solvates, respectively. The phenylborane-bridged tetrahydrocarbazole core in all three structures is generally planar, showing a slight cupping angle between the pyrrole rings (6.33(13)–7.77(6)°). The fused cyclohexene ring of the tetrahydrocarbazole adopts a half-chair conformation in all cases. In the structure where the cyclohexene ring is substituted, **SpAc-DtButHCzB**, the C3 carbon of the tetrahydrocarbazole moiety is oriented either above or below the plane, with the *tert*-butyl group in a pseudo-equatorial position. For both **SpAc-DtButHCzB** and **SpAc-tButHCzB**, the acridine unit is oriented approximately perpendicularly to the central benzene ring (angle between benzene and acridine central ring 80.10(6) and 83.46(9)°, respectively), with the acridine itself bent (angle between benzene rings of each acridine 14.88(7) and 22.19(10)°, respectively), and the fluorene unit is arranged nearly orthogonal (angle between central rings of acridine and fluorene 87.13(8) and 88.79(10)°, respectively).

In the structures of **tButHCzB** and **SpAc-DtButHCzB**, the planar fused ring systems stack face-to-face (centroid···centroid 3.5304(10) and 3.7983(16)°, respectively) (Fig. 2), with **SpAc-DtButHCzB** showing additional edge-to-face packing between adjacent spiro-acridine moieties (Fig. 2(a)) (centroid···H

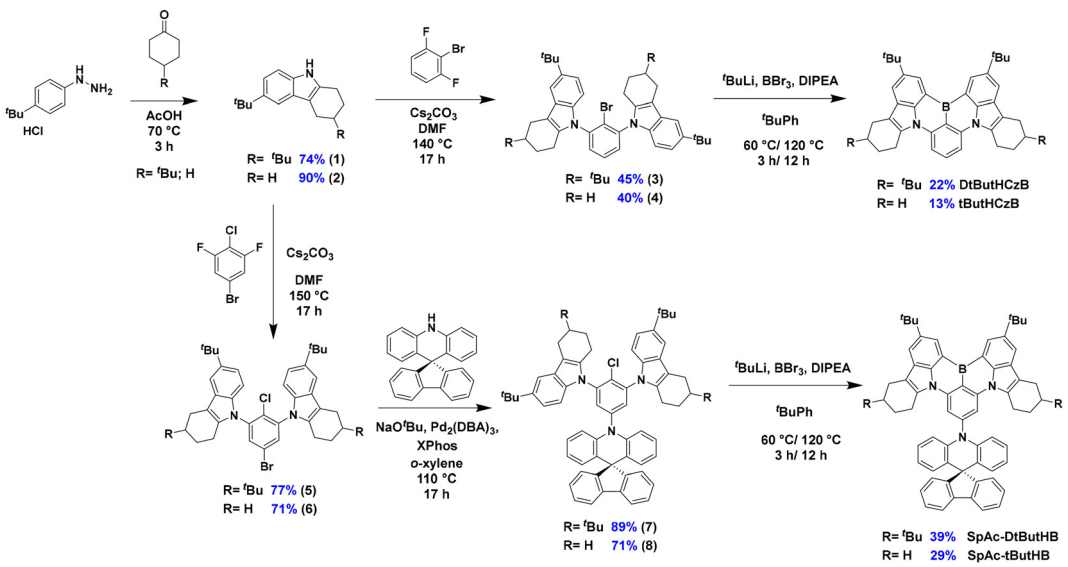

Scheme 1 Synthesis of **tButHCzB**, **DtButHCzB**, **SpAc-tButHCzB**, and **SpAc-tButHCzB**.

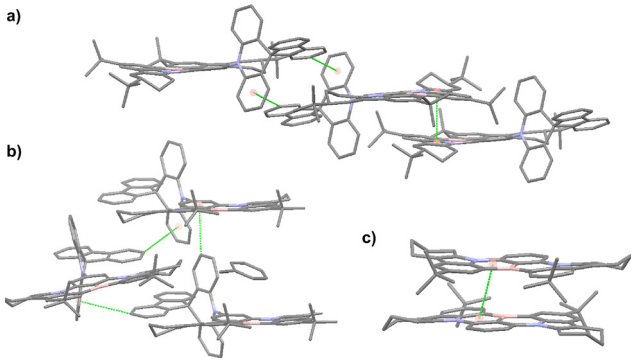

Fig. 2 Face-to-face and edge-to-face (green dashed lines) stacking in the crystal structures of (a) **SpAc-DtButHCzB**, (b) **SpAc-tButHCzB**, and (c) **tButHCzB**. Hydrogen atoms, minor parts of disorder, and solvates (except for one toluene in **SpAc-tButHCzB**) are omitted for clarity.

2.6758(8) Å). Edge-to-face packing is prevalent in the packing of **SpAc-tButHCzB** with the spiro-acridine moieties forming interactions to both the fused ring core and adjacent spiro-acridines (centroid···H 2.6938(11) and 3.0051(12) Å, respectively), while the toluene solvents occupy the space (plane···plane 7.238(6) Å) between coplanar molecules (Fig. 2(b)). Face-to-face packing arrangements are generally considered unfavourable for light-emitting materials, as π–π interactions can promote non-radiative decay pathways, thereby reducing the photoluminescence quantum yield (Φ_{PL}). The observed packing in **tButHCzB** and **SpAc-DtButHCzB** indicates potentially strong π–π interactions, which are expected to contribute to aggregation-caused quenching. While the structure of **SpAc-tButHCzB** does not adopt a face-to-face alignment, this may be a result of inclusion of the toluene solvate between parallel-aligned **SpAc-tButHCzB** molecules. As such the **tButHCz** moieties could still facilitate aggregation and increase non-radiative decay in the solid state.[21]

Theoretical calculations

We undertook a computational study to understand the impact of saturation of the carbazole donor on the optoelectronic properties, first evaluating the ground-state geometry and orbital energies at the PBE0/6-31G(d,p) level of theory[22] using a toluene solvent polarity field. The predicted HOMO and LUMO energy levels for **DtButHCzB** and **tButHCzB** are −5.28/−5.29 eV and −1.66/−1.67 eV and for **SpAc-DtButHCzB** and **SpAc-tButHCzB** are −5.36/−5.35 eV and −1.81/−1.80 eV (Fig. 3). The predicted stabilization of the HOMO and especially the LUMO levels for the donor-substituted derivatives is an unexpected anomaly, since the presence of the donor should mesomerically interact with the boron acceptor and lead to a destabilization of both the HOMO and especially the LUMO; this behavior was also predicted at both the PBE0/6-31G(d,p) and M06-2X/6-31G(d,p) levels in the gas phase (Fig. S5 and S6). This is in contrast to **DtBuCzB** (HOMO = −5.06 eV; LUMO = −1.71 eV)[23] and **tDPA-DtCzB** (HOMO = −4.93 eV; LUMO = −1.55 eV)[23] where there is a predicted destabilization of both the HOMO and LUMO with donor substitution *para* to the boron atom. Both **DtButHCzB** and **tButHCzB** are thus predicted to have larger HOMO–LUMO gaps (ΔE) of 3.62 eV, while **SpAc-DtButHCzB** and **SpAc-tButHCzB** are predicted to have smaller ΔE of 3.45 eV each. In comparison to the structurally related compounds **DtBuCzB** and **TMInBN** (both having ΔE = 3.66 eV), **DtButHCzB** and **tButHCzB** have a modestly smaller ΔE.

It has been shown that TD-DFT calculations do not provide accurate predictions for the energies of the low-lying excited states nor for the energy gap between S_1 and T_1 (ΔE_{ST}) for compounds that possess an SRCT emissive S_1 state.[24] Therefore, we computed the energies of the excited states at the RI-wPBEPP86/cc-pVDZ level of theory (Fig. 3(b)), which has been demonstrated to provide comparable accuracy to high-level coupled cluster calculations.[25,26] Double-hybrid density functional methods were employed in this study, as coupled cluster calculations were found to be computationally too demanding due to the molecular flexibility and the number of heavy atoms in these compounds. These calculations predict similar S_1 and T_1 levels of 3.18/3.19 eV and 2.93/2.93 eV for **DtButHCzB** and **tButHCzB**, respectively. This results in moderate ΔE_{ST} values of 0.25 and 0.26 eV, respectively. A high oscillator strength, *f*, of 0.51 and 0.49 is predicted for **DtButHCzB** and **tButHCzB**, respectively, suggesting that these two compounds will have high Φ_{PL}. The S_1 and T_1 energy levels of **SpAc-DtButHCzB** and **SpAc-tButHCzB** show similarly close values to each other at 3.15/3.15 eV and 2.88/2.89 eV, respectively. Both S_1 and T_1 are stabilized in **SpAc-DtButHCzB** and **SpAc-tButHCzB** as compared to **DtButHCzB** and **tButHCzB**, and their ΔE_{ST} and *f* values are comparable at 0.26 and 0.27 eV, and 0.48 and 0.50, respectively. All four emitters possess T_2 and T_3 states that are slightly higher in energy than their corresponding S_1 states. It has been shown that higher-lying triplet states that are close in energy to S_1 can participate in the reverse intersystem crossing (RISC) process and promote TADF in compounds with seemingly large ΔE_{ST}.[27] Difference density plots show the expected alternating pattern between density gain (yellow) and density loss (blue) for MR-TADF emitters that indicate the SRCT character of these emitters (Fig. 3(b)). For **SpAc-tButHCzB** and **SpAc-DtButHCzB**, the higher lying excited states S_2, S_3 and T_2 and T_3 are not predicted to possess LRCT character between the spiro-acridine (donor) and the MR-TADF core (acceptor) (Table S3). When compared to the unsaturated reference **DtBuCzB**[18] (S_1 = 3.14 eV; T_1 = 3.02 eV; ΔE_{ST} = 0.12 eV calculated at the same level of theory), **DtButHCzB** and **tButHCzB** are predicted to show a blue-shifted emission and larger ΔE_{ST} (Fig. S7). By contrast, a decrease in S_1 energy is predicted compared to the structurally related **TMInBN**[16] (S_1 = 3.26 eV; T_1 = 2.94 eV; ΔE_{ST} = 0.32 eV calculated at the same level of theory, Fig. S7). This stabilization can be assigned to the relatively stronger donating strength (shallower HOMO level) of the tetrahydrocarbazole derivatives as compared to the dimethylindole donor used in **TMInBN** (Table S2). However, the T_1 energy levels for **tButHCzB** and **DtButHCzB** (both 2.93 eV) are comparable to that of **TMInBN** (T_1 = 2.94 eV), resulting in a smaller ΔE_{ST}, which is expected to lead to more efficient TADF (Fig. S7). A similar trend is observed for the donor-decorated congeners **SpAc-DtButHCzB** and

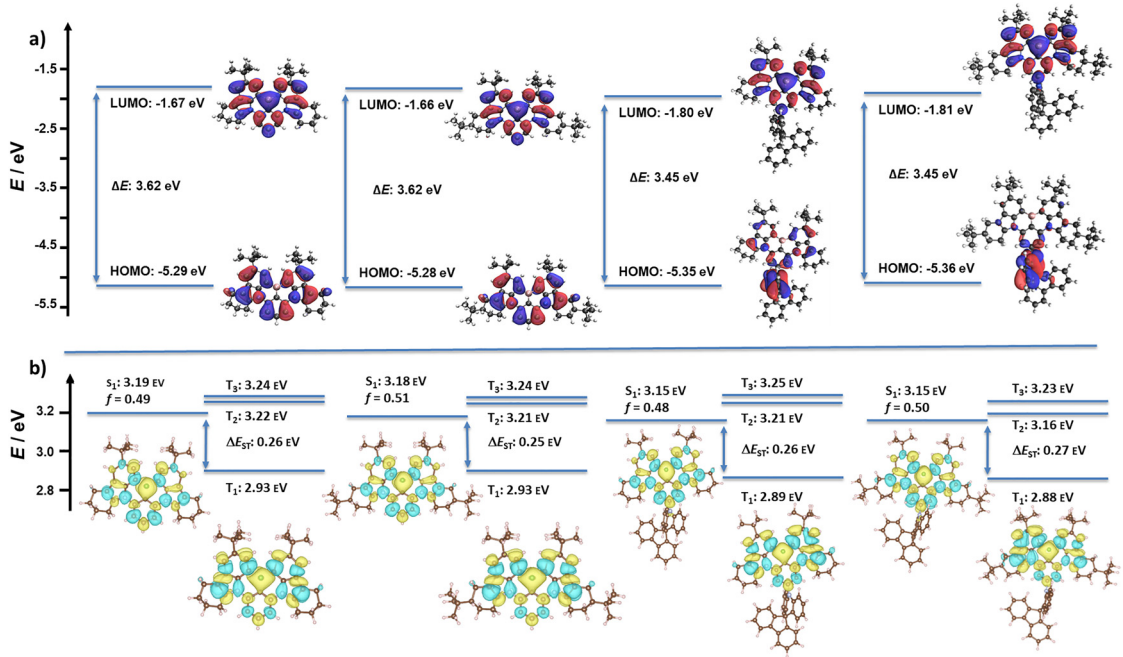

Fig. 3 Theoretical calculations (a) HOMO and LUMO energy level and orbital density plots (iso value 0.02) at the PBE0/6-31G(d,p) (toluene) level of theory. (b) Excited-state energy levels calculated at the RI-wPBEPP86/cc-pVDZ level of theory in the gas phase and corresponding difference density plots (yellow = positive; blue = negative; isovalue 0.001).

SpAc-tButHCzB as compared to their unsaturated counterpart **SpAc-tCzBN**[19,20] (S_1 = 3.11 eV; T_1 = 3.07 eV; ΔE_{ST} = 0.04 eV calculated at the same level of theory, Fig. 1) where the S_1 states in the former two are destabilized while their T_1 states are stabilized. Therefore, **SpAc-DtButHCzB** and **SpAc-tButHCzB** are predicted to possess much larger ΔE_{ST} of 260 and 270 meV, respectively, as compared to **SpAc-tCzBN** (Fig. S8).

Photophysical properties

We first investigated the photophysical properties of all four emitters in dilute toluene solutions ($\sim 10^{-6}$ M) (Table 1). Their absorption spectra possess a sharp, intense, lowest energy absorption band associated with the S_0–S_1 SRCT transition peaking at λ_{abs} of 467, 468, 464 and 465 nm, with associated molar extinction coefficients, ε, of 44, 44, 47, 47 $\times$ 10^4 M^{-1} cm^{-1} for **tButHCzB**, **DtButHCzB**, **SpAc-tButHCzB** and **SpAc-DtButHCzB**, respectively (Fig. 4(a)). There is a small hypsochromic shift of this absorption band for the donor decorated derivatives, **SpAc-tButHCzB** and **SpAc-DtButHCzB** that is consistent with their slightly larger ΔE (Table 3). The SRCT bands of these four saturated analogues are of similar energy compared to their respective bands in the unsaturated counterparts, **DtBuCzB** and **SpAc-tCzBN**. The four compounds have small Stokes shifts of around 12 nm and narrowband emission (FWHM, of 21, 21, 19, and 18 nm) that are reflective of their rigid structures. The PL

Table 1 Photophysical properties

Compound	Medium	$\lambda_{abs}(\varepsilon)^c$/nm ($10^4$ M^{-1} cm^{-1})	$\lambda_{PL}{}^d$/nm	FWHM^e/nm	$E_{S_1}{}^f$/eV	$E_{T_1}{}^g$/eV	$\Delta E_{ST}{}^h$/eV	$\Phi_{PL}{}^i$/%	$\tau_p{}^j$/ns	$\tau_d{}^k$/ms
tButHCzB	Sol.^{a}	467 (35)	479	21	2.62	2.30	0.32	91/76	7.5	—
	Film^b		491	45	2.65	2.34	0.31	61/42	5.3	95
DtButHCzB	Sol.^{a}	468 (39)	480	21	2.61	2.30	0.31	87/69	7.1	—
	Film^b		490	34	2.63	2.31	0.32	57/45	5.5	154
SpAc-tButHCzB	Sol.^{a}	464 (44)	476	19	2.66	2.29	0.37	86/69	7.2	—
	Film^b		483	27	2.67	2.32	0.35	53/43	5.2	108
SpAc-DtButHCzB	Sol.^{a}	465 (47)	477	18	2.64	2.26	0.35	90/77	6.2	—
	Film^b		483	26	2.66	2.31	0.35	53/44	6.3	148

^{a} In dilute toluene solution ($\sim 10^{-6}$ M). λ_{exc} = 380 nm. ^{b} Spin-coated thin films of 1 wt% emitter in mCP. λ_{exc} = 340 nm. ^{c} Lowest energy absorbance peak; molar extinction coefficient ε in parentheses. ^{d} PL maximum. ^{e} Full-width half maximum of the emission band. ^{f} S_1 energy level determined from the onset of the steady-state PL spectrum in 2-MeTHF glass at 77 K. λ_{exc} = 380 nm. ^{g} T_1 energy level determined from the onset of the time-gated emission spectra (10–85 ms) in 2-MeTHF glass at 77 K. λ_{exc} = 380 nm. ^{h} $\Delta E_{ST} = E_{S_1} - E_{T_1}$. ^{i} Photoluminescence quantum yield; absolute Φ_{PL} of the thin films was measured using an integrating sphere; relative Φ_{PL} in solutions was measured by a comparative method using quinine sulfate as the reference (Φ_r = 54.6% in 1 N H_2SO_4).[35] ^{j} Prompt lifetimes were measured by TCSPC with a 200 ns time window. λ_{exc} = 375 nm. ^{k} Delayed lifetimes were measured by MCS with a 1 s time window. λ_{exc} = 340 nm.

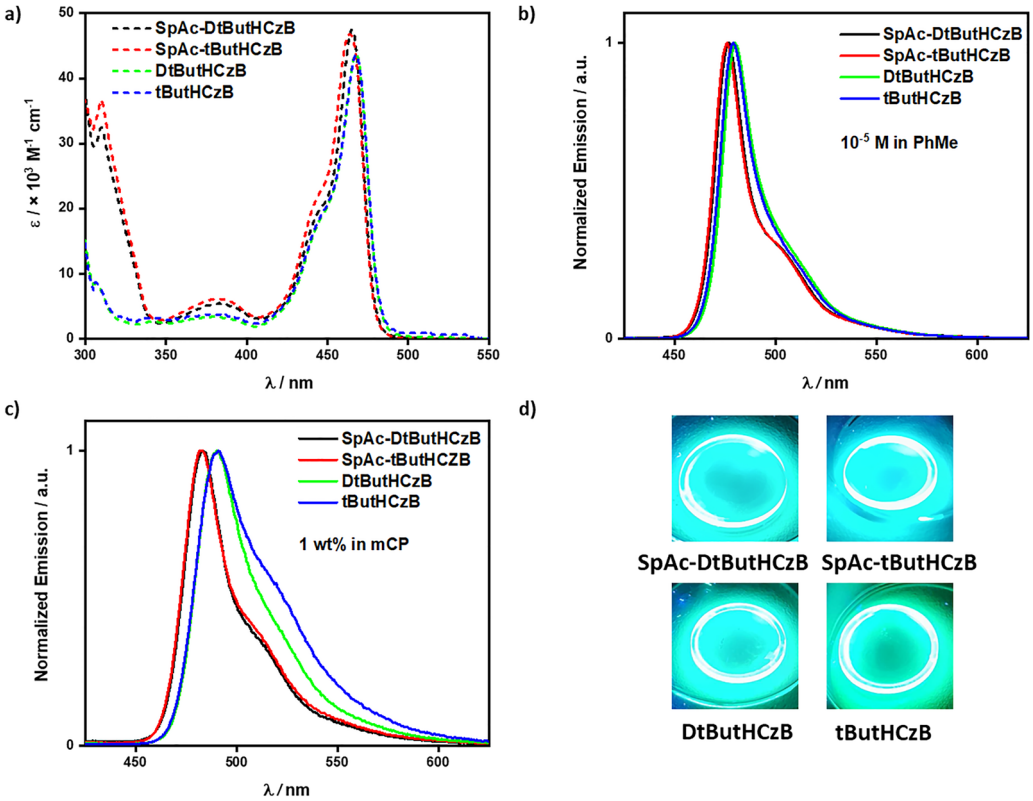

Fig. 4 (a) Molar absorptivity in dilute toluene solution (10^{-6} M). (b) Steady-state PL spectra in dilute toluene solution (10^{-6} M; λ_{exc} = 380 nm). (c) Steady-state PL spectra of 1 wt% doped films in mCP (λ_{exc} = 340 nm). (d) Photos of spin-coated films under UV-irradiation of **SpAc-DtButHCzB**, **SpAc-tButHCzB**, **DtButHCzB** and **tButHCzB**.

peaks at λ_{PL} of 479, 480, 476, and 477 nm for **tButHCzB**, **DtButHCzB**, **SpAc-tButHCzB**, and **SpAc-DtButHCzB**, respectively (Fig. 4(b)). Solvatochromism studies of the absorption and PL confirmed the SRCT character of the emissive excited state in all four derivatives (Fig. S11 and S12).

Time-resolved photoluminescence (TRPL) measurements in degassed toluene solution (10^{-6} M) reveal no delayed emission, which is not unusual for MR-TADF compounds possessing moderately large ΔE_{ST}.[28–31] The PL lifetimes, τ_{PL}, are 7.2, 6.2, 7.5, and 7.1 ns for **SpAc-tButHCzB**, **SpAc-DtButHCzB tButHCzB**, and **DtButHCzB**, respectively. In degassed toluene solution **tButHCzB**, **DtButHCzB**, **SpAc-tButHCzB** and **SpAc-DtButHCzB** have high Φ_{PL} of 91, 87, 86, and 90%, which decrease to 76, 69, 69, and 77% in air, respectively. This decrease under aerated conditions points to accessible triplet states involved in the emission mechanism. However, delayed emission is too weak to detect due to competing non-radiative decay and the inefficient population of the triplet excited states.

The S_1 and T_1 levels were determined from the onsets of the steady-state PL and time-gated emission spectra, respectively, in 2-methyltetrahydrofuran (2-MeTHF) glass at 77 K (Table 2 and Fig. 4). The S_1 levels increase narrowly from **DtButHCzB** (2.61 eV) to **SpAc-tButHCzB** (2.66 eV). There is a clear structure–property trend observed, where both decreasing the number of *tert*-butyl groups from four to two and introducing the acridine donor moiety introduces a small destabilization of the S_1 energy level, while the T_1 level remains unaffected by the number of *tert*-butyl groups (T_1 = 2.30 eV for **DtButHCzB** and **tButHCzB**). There is only a small stabilization of the T_1 energy in the derivatives containing the spiro-acridine donor (T_1 = 2.29 eV for **SpAc-DtButHCzB** and **SpAc-tButHCzB**). The trend in T_1 energies is well reproduced by the double hybrid calculations, while the trend in S_1 levels is only partially captured by the computations, which incorrectly predict a stabilization of the S_1 state in the donor-decorated derivatives. When compared to the structurally related emitter **DtBuCzB** (S_1 = 2.66 eV; T_1 = 2.53 eV in frozen toluene),[18] the measured S_1 and T_1 energies for **DtButHCzB** and **tButHCzB** are both stabilized. This red-shift can be reasonably attributed to the reduced polarity of the toluene host matrix compared to the 2-MeTHF host matrix employed in this study. Notably, the S_1 energies of **SpAc-DtButHCzB** and **SpAc-tButHCzB** are comparable with their

Table 2 Rate constants of **tButHCzB**, **DtButHCzB**, **SpAc-tButHCzB** and **SpAc-DtButHCzB**

Compound	$k_r/\times10^7$ s^{-1}	$k_{nr}/\times10^7$ s^{-1}	$k_{ISC}/\times10^8$ s^{-1}	$k_{RISC}/\times10$ s^{-1}
tButHCzB	5.94	3.80	3.60	1.44
DtButHCzB	1.77	1.33	1.10	2.95
SpAc-tButHCzB	4.31	3.38	1.15	2.31
SpAc-DtButHCzB	3.00	2.66	1.02	1.89

unsaturated analogue **SpAc-tCzBN** (S_1 = 2.64 eV; T_1 = 2.49 eV in frozen toluene),[19] even though the latter was measured in a less polar environment. Interestingly, the T_1 energy of the reference compound **SpAc-tCzBN** is approximately 0.2 eV higher than those measured for **SpAc-DtButHCzB** and **SpAc-tButHCzB**. The ΔE_{ST} values are 320, 310, 370, and 350 eV for **tButHCzB**, **DtButHCzB**, **SpAc-tButHCzB**, and **SpAc-DtButHCzB**, respectively. These ΔE_{ST} represent a large barrier for direct RISC from T_1 to S_1, but one that is not impossible to overcome, given literature examples with similarly large ΔE_{ST} values yet nonetheless show TADF behavior.[32–34]

As 1 wt% doped films in mCP, a host with a suitably high triplet energy (2.90 eV),[36] the PL spectra of **SpAc-tButHCzB** and **SpAc-DtButHCzB** are bathochromically shifted and broadened at λ_{PL} of 483 nm for both (FWHM of 27 and 26 nm; Fig. 4(c)), respectively, compared to those in toluene. The PL spectra of **tButHCzB** and **DtButHCzB** show an even larger red-shift and broadening to λ_{PL} of 491 and 490 nm (FWHMs of 45 and 34 nm), respectively. This observed red-shift and broadening of the emission band indicates that these molecules have a strong tendency to aggregate, which becomes even more pronounced at higher doping concentrations (Fig. S17). The observed aggregation is likely caused by the formation of π–π stacked dimers, as observed in the crystal structures, even for doping concentrations as low as 1 wt%. Additionally, the Φ_{PL} values of 53–61% represent a significant decrease compared to the solution-state measurements (Φ_{PL} of 86–91%, Table 2), this is consistent with these compounds aggregating. This behavior is consistent across a range of host materials of varying steric bulk and polarity (Fig. S18 and Table S4), underlining the intrinsic tendency to form aggregates in the solid state. This aggregation and the subsequent ACQ may be caused by the formation of H-bonds in the solid state, increasing the reorganisation energy due to the contribution from C–H stretching vibrational modes.[37,38] The S_1 and T_1 energy levels were determined from the onset of the steady-state and time-gated PL spectra at 77 K. For **SpAc-DtButHCzB** and **SpAc-tButHCzB** the S_1 levels were found to be 2.66 and 2.67 eV, respectively. The T_1 levels were 2.31 and 2.32 eV for **SpAc-DtButHCzB** and **SpAc-tButHCzB**, respectively. These values result in ΔE_{ST} of 350 meV for both **SpAc-DtButHCzB** and **SpAc-tButHCzB** and slightly smaller values of 320 and 310 meV for **DtButHCzB** and **tButHCzB**, respectively. As observed in frozen 2-MeTHF, the time-gated PL (10–85 ms) spectra of the films show residual delayed fluorescence in addition to phosphorescence (Fig. S14). The TRPL measurements under vacuum reveal that the PL of all four emitters decays with prompt lifetimes in the range of 5.2–6.3 ns, which are of similar magnitude to the solution-state measurements. In TRPL multichannel scaling experiment long delayed components were found with lifetimes, τ_d, of 148, 108, 154 and 95 ms for **SpAc-DtButHCzB**, **SpAc-tButHCzB**, **DtButHCzB** and **tButHCzB**, respectively. Compared to their

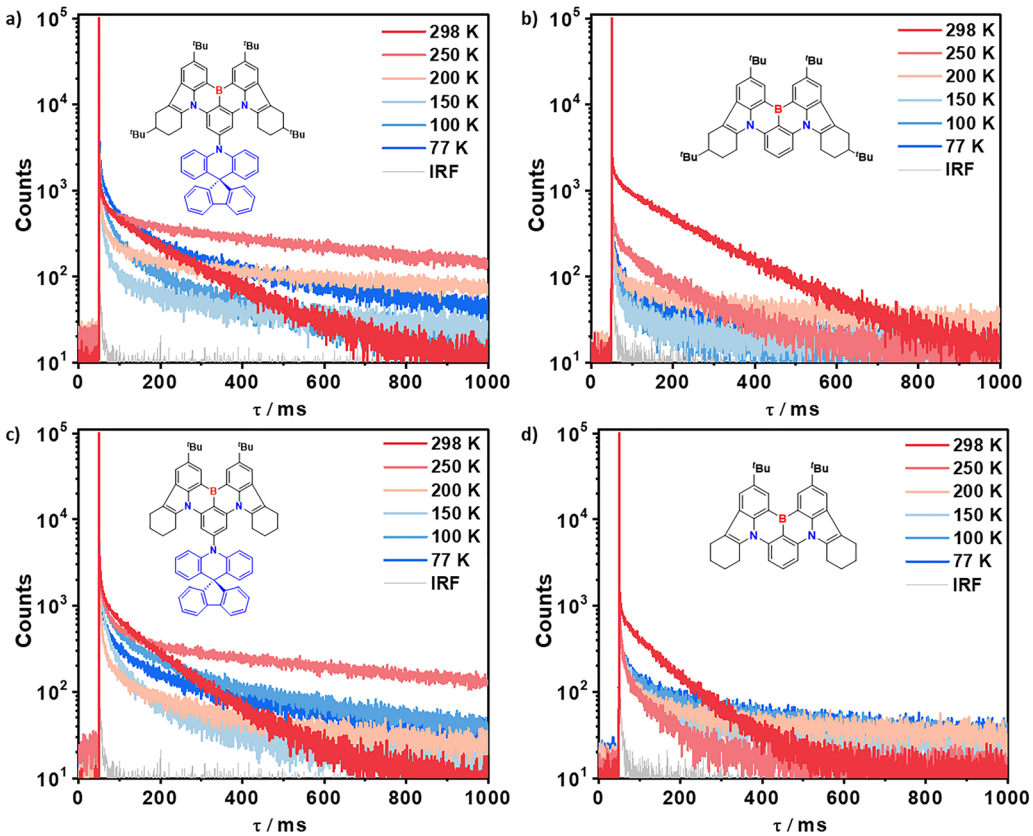

Fig. 5 Temperature-dependent TRPL decays of 1 wt% doped films in mCP of (a) **SpAc-DtButHCzB**, (b) **DtButHCzB**, (c) **SpAc-tButHCzB** and (d) **tButHCzB**; (λ_{exc} = 340 nm).

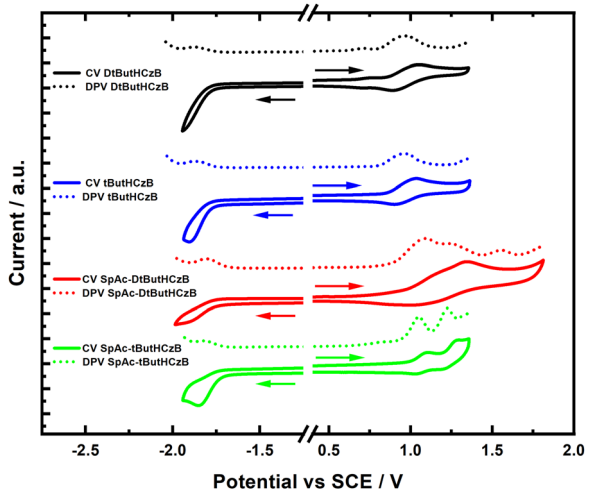

Fig. 6 Cyclic voltammetry (CV) and different pulse voltammetry (DPV) measurements performed in DCM solution (0.1 M [^{n}Bu$_4$N]PF$_6$) at a scan rate of 0.1 V s^{-1} and referenced to SCE ($E_{ox/red}$ [V *vs.* SCE] = $E_{ox/red}$ [V *vs.* Fc/Fc$^+$] + 0.46).[39]

unsaturated analogues **DtBuCzB** (69 μs; in mCBP)[18] and **SpAc-tCzBN** (45 μs; 10 wt% in PhCzBCz)[19] the PL of the tetrahydrocarbazole based emitters decays with a much longer lifetime, which is due to the comparably larger ΔE_{ST} in these compounds. Temperature-dependent TRPL measurements (Fig. 5) confirmed the TADF character of the four compounds. For the SpAc-extended emitters, **SpAc-DtButHCzB** and **SpAc-tButHCzB**, there is a very long lived emission at low temperatures (Fig. 5(a) and (c)), which is assigned to phosphorescence, while for **DtButHCzB** and **tButHCzB** (Fig. 5(b) and (d)) the delayed emission component of the TRPL significantly decreases at temperatures below room temperature, due to insufficient thermal energy to overcome the large ΔE_{ST}.

A comparison of the rate constants reveals that **SpAc-DtButHCzB** and **DtButHCzB** exhibit slower reverse intersystem crossing rates (k_{RISC}) compared to those with only two *tert*-butyl groups (**tButHCzB** and **SpAc-tButHCzB**). This suggests that the additional bulky substituents may hinder RISC. At the same time **SpAc-DtButHCzB** and **DtButHCzB** also display reduced non-radiative decay rates. Radiative decay rates (k_r) are generally comparable across the four emitters, indicating that prompt fluorescence is not significantly affected by the substitution.

Electrochemistry

The electrochemical properties were investigated in DCM with 0.1 M [^{n}Bu$_4$N]PF$_6$ as the supporting electrolyte using ferrocene/ferrocenium (Fc/Fc$^+$) as an internal standard. The potentials are referenced to SCE ($E_{ox/red}$ [V *vs.* SCE] = $E_{ox/red}$ [V *vs.* Fc/Fc$^+$] + 0.46).[39] All four emitters possess similar oxidation (E_{ox}) and reduction (E_{red}) potentials in DCM, ranging from 0.96 to 1.08 V and −1.81 to −1.88 V, respectively (Fig. 6 and Table 3). All measured electrochemical processes are irreversible. Compounds **SpAc-DtButHCzB** and **SpAc-tButHCzB** have anodically shifted E_{ox} and E_{red} values compared to those of **DtButHCzB** and **tButHCzB**, in line with the calculated values. The HOMO and LUMO levels were inferred from the E_{ox}/E_{red} values using the relationship $E_{HOMO/LUMO} = -(E_{ox/red} + 4.8\ eV)$.[40] The corresponding HOMO levels of **SpAc-DtButHCzB** and **SpAc-tButHCzB** are −5.42 and −5.39 eV, respectively. **DtButHCzB** and **tButHCzB** have shallower HOMO levels at −5.31 and −5.30 eV, respectively. A similar trend is observed for the LUMO energy levels, with a value of −2.47 eV for both **DtButHCzB** and **tButHCzB**, while **SpAc-DtButHCzB** and **SpAc-tButHCzB** have stabilized values of −2.53 and −2.52 eV, respectively. It is evident that the presence of the additional *tert*-butyl groups in **SpAc-DtButHCzB** and **DtButHCzB** stabilizes the HOMO, while the LUMO remains unaffected. The corresponding ΔE values are larger for **SpAc-DtButHCzB** and **SpAc-tButHCzB** than for **DtButHCzB** and **tButHCzB**, which results from the stronger stabilization of the HOMO compared to the LUMO in the former two compounds. This highlights again the above-mentioned theoretical calculation anomaly, since the predicted ΔE (Table 3) is smaller for **SpAc-tButHCzB** and **SpAc-DtButHCzB**, than for their unsaturated parent emitters, **tButHCzB** and **DtButHCzB**.

Conclusions

In this study we explored an approach to decrease the conjugation length and planarity of the donor fragment used in MR-TADF emitters in order to blue-shift the emission. Partially saturating the carbazole donor also positively improved the solubility of these compounds. The four emitters in this study all have very high Φ_{PL} in solution and emit in the sky-blue region, showing very narrowband PL spectra. Unfortunately, in the solid state, these molecules showed a strong tendency to aggregate, even at low doping concentrations, and this resulted in a significant drop in their Φ_{PL} values, which rendered their

Table 3 Electrochemistry data obtained by DPV measurements in DCM solution (0.1 M [^{n}Bu$_4$N]PF$_6$)

Compound	E_{ox}[a]/eV	HOMO exp.[b]/eV	HOMO calc.[c]/eV	E_{red}[d]/eV	LUMO exp.[e]/eV	LUMO calc.[f]/eV	ΔE exp[g]/eV	ΔE calc.[g]/eV
tButHCzB	0.96	−5.30	−5.29	−1.87	−2.47	−1.67	2.83	3.62
DtButHCzB	0.97	−5.31	−5.28	−1.88	−2.47	−1.66	2.84	3.62
SpAc-tButHCzB	1.05	−5.39	−5.35	−1.82	−2.52	−1.80	2.87	3.54
SpAc-DtButHCzB	1.08	−5.42	−5.36	−1.81	−2.53	−1.81	2.89	3.55

[a] Oxidation potential *vs.* SCE obtained by DPV measurements with a scan rate of 0.1 V s^{-1} and referenced to SCE($E_{ox/red}$ [V *vs.* SCE] = $E_{ox/red}$ [V *vs.* Fc/Fc$^+$] + 0.46).[39] [b] HOMO = $-(E_{ox,Fc/Fc^+} + 4.8\ eV)$. [c] Calculated HOMO energy level on PBE0/6-31G(d,p) (toluene) level. [d] E_{red} *vs.* SCE obtained by DPV measurements with a scan rate of 0.1 V s^{-1} and referenced to SCE ($E_{ox/red}$ [V *vs.* SCE] = $E_{ox/red}$ [V *vs.* Fc/Fc$^+$] + 0.46).[39] [e] LUMO = $-(E_{red,Fc/Fc^+} + 4.8\ eV)$. [f] Calculated LUMO energy level at the PBE0/6-31G** (toluene) level. [g] ΔE = |(HOMO–LUMO)|.

use as emitters in OLEDs not desirable. Nonetheless, this work highlights a robust structure–property study that explores new chemical space in MR-TADF emitter design. The design concept was successful in that the emission was blue-shifted as a result of partial saturation of the carbazole donors. Current efforts are focused on derivatizing these compounds to mitigate the strong quenching in the solid state and recover the high Φ_{PL} observed in solution.

Author contributions

M. F.: conceptualization, data curation, formal analysis, investigation, methodology, visualization, writing – original draft preparation, writing – review & editing. A. P. M.: data curation, formal analysis, investigation, visualization, writing – review & editing. D. B. C.: writing – review & editing. E. Z.-C.: conceptualization, funding acquisition, methodology, project administration, resources, supervision, writing – review & editing.

Conflicts of interest

There are no conflicts to declare.

Data availability

The research data supporting this publication can be accessed at **https://doi.org/10.17630/ba2c5474-135e-4b6e-84d4-74980f549178**.

Supplementary information: ^{1}H NMR and ^{13}C NMR spectra, HRMS, and elemental analysis; details of X-ray crystallography; supplementary computational data and coordinates; supplemental photophysical data. see DOI: **https://doi.org/10.1039/d5tc02496j**.

CCDC 2465301, 2465303 and 2465304 contain the supplementary crystallographic data for this paper.[41a–c]

Acknowledgements

This project has been funded by the European Union Horizon 2021 research and innovation programme under grant agreement no. 101073045 (TADFsolutions). We thank the EPSRC for support (EP/X026175/1, EP/W015137/1, EP/R00188X/1, EP/W007517/1, and EP/Z535291/1). We thank Aminata Mariko for her help with the synthesis of the tetrahydrocarbazole derivatives.

References

1 J. M. Dos Santos, D. Hall, B. Basumatary, M. Bryden, D. Chen, P. Choudhary, T. Comerford, E. Crovini, A. Danos, J. De, S. Diesing, M. Fatahi, M. Griffin, A. K. Gupta, H. Hafeez, L. Hammerling, E. Hanover, J. Haug, T. Heil, D. Karthik, S. Kumar, O. Lee, H. Li, F. Lucas, C. F. R. Mackenzie, A. Mariko, T. Matulaitis, F. Millward, Y. Olivier, Q. Qi, I. D. W. Samuel, N. Sharma, C. Si, L. Spierling, P. Sudhakar, D. Sun, E. Tankeleviciu Te, M. Duarte Tonet, J. Wang, T. Wang, S. Wu, Y. Xu, L. Zhang and E. Zysman-Colman, *Chem. Rev.*, 2024, **124**(24), 13736.
2 S. Madayanad Suresh, D. Hall, D. Beljonne, Y. Olivier and E. Zysman-Colman, *Adv. Funct. Mater.*, 2020, **30**(33), 1616.
3 Q. He, M. Li and S. J. Su, *ChemPhysChem*, 2025, **26**(7), e202400955.
4 M. Du, J. Zhou, X. Luo, L. Duan and D. Zhang, *Moore and More*, 2024, **1**(1), 3004.
5 E. Tankeleviciute, I. D. W. Samuel and E. Zysman-Colman, *J. Phys. Chem. Lett.*, 2024, **15**(4), 1034.
6 B. Cui, J. Zhou, C. Duan and H. Xu, *Adv. Opt. Mater.*, 2025, 2403295.
7 J. Y. Woo, M. H. Park, S. H. Jeong, Y. H. Kim, B. Kim, T. W. Lee and T. H. Han, *Adv. Mater.*, 2023, **35**(43), e2207454.
8 T. W. Lee, T. Noh, H. W. Shin, O. Kwon, J. J. Park, B. K. Choi, M. S. Kim, D. W. Shin and Y. R. Kim, *Adv. Funct. Mater.*, 2009, **19**(10), 1625.
9 L. Duan, L. Hou, T.-W. Lee, J. Qiao, D. Zhang, G. Dong, L. Wang and Y. Qiu, *J. Mater. Chem.*, 2010, **20**(31), 6392.
10 *Nat. Photonics*, 2009, **3**(8), 441, **https://www.nature.com/articles/nphoton.2009.133.pdf**.
11 C. M. Cole and S. D. Yambem, *Adv. Opt. Mater.*, 2024, **13**(1), 2402019.
12 D. Hall, S. M. Suresh, P. L. dos Santos, E. Duda, S. Bagnich, A. Pershin, P. Rajamalli, D. B. Cordes, A. M. Z. Slawin, D. Beljonne, A. Köhler, I. D. W. Samuel, Y. Olivier and E. Zysman-Colman, *Adv. Opt. Mater.*, 2019, **8**(2), 1901627.
13 Y. Yuan, X. Tang, X. Y. Du, Y. Hu, Y. J. Yu, Z. Q. Jiang, L. S. Liao and S. T. Lee, *Adv. Opt. Mater.*, 2019, **7**(7), 1801536.
14 T. Hatakeyama, K. Shiren, K. Nakajima, S. Nomura, S. Nakatsuka, K. Kinoshita, J. Ni, Y. Ono and T. Ikuta, *Adv. Mater.*, 2016, **28**(14), 2777.
15 L. Wu, X. Mu, D. Liu, W. Li, D. Li, J. Zhang, C. Liu, T. Feng, Y. Wu and J. Li, *et al.*, *Angew. Chem., Int. Ed.*, 2024, **63**(38), e202409580.
16 C.-Z. Du, Y. Lv, H. Dai, X. Hong, J. Zhou, J.-K. Li, R.-R. Gao, D. Zhang, L. Duan and X.-Y. Wang, *J. Mater. Chem. C*, 2023, **11**(7), 2469.
17 Y. T. Lee, C. Y. Chan, M. Tanaka, M. Mamada, U. Balijapalli, Y. Tsuchiya, H. Nakanotani, T. Hatakeyama and C. Adachi, *Adv. Electron. Mater.*, 2021, **7**(4), 2001090.
18 Y. Xu, Z. Cheng, Z. Li, B. Liang, J. Wang, J. Wei, Z. Zhang and Y. Wang, *Adv. Opt. Mater.*, 2020, **8**(9), 1902142.
19 X. Song, S. Shen, S. Zou, F. Guo, Y. Wang, S. Gao and Y. Zhang, *Chem. Eng. J.*, 2023, **467**, 143557.
20 Q. Wu, J. Li, D. Liu, Y. Mei, B. Liu, J. Wang, M. Xu and Y. Li, *Dyes Pigm.*, 2023, **217**, 111421.
21 N. J. Silva, F. B. Machado, H. Lischka and A. J. Aquino, *Phys. Chem. Chem. Phys.*, 2016, **18**(32), 22300.
22 D. Hall, J. C. Sancho-Garcia, A. Pershin, D. Beljonne, E. Zysman-Colman and Y. Olivier, *J. Phys. Chem. A*, 2023, **127**(21), 4743.
23 X. Yan, Z. Li, Q. Wang, Y. Qu, Y. Xu and Y. Wang, *J. Mater. Chem. C*, 2022, **10**(41), 15408.
24 D. Hall, J. C. Sancho-Garcia, A. Pershin, G. Ricci, D. Beljonne, E. Zysman-Colman and Y. Olivier, *J. Chem. Theory Comput.*, 2022, **18**(8), 4903.

25 T. Schwabe and S. Grimme, *Phys. Chem. Chem. Phys.*, 2007, **9**(26), 3397.
26 M. Kondo, *Chem. Phys. Lett.*, 2022, **804**, 139895.
27 Z. Huang, H. Xie, J. Miao, Y. Wei, Y. Zou, T. Hua, X. Cao and C. Yang, *J. Am. Chem. Soc.*, 2023, **145**(23), 12550.
28 L. Yang, L. Dong, D. Hall, M. Hesari, Y. Olivier, E. Zysman-Colman and Z. Ding, *SmartMat*, 2022, **4**(2), 1149.
29 T. J. Penfold, F. B. Dias and A. P. Monkman, *Chem. Commun.*, 2018, **54**(32), 3926.
30 J. Wang, Y. Yasuda, Y. Ren, R. Kondo, D. B. Cordes, H. Kaji and E. Zysman-Colman, *Org. Chem. Front.*, 2025, **12**(10), 3279.
31 X. Wu, B.-K. Su, D.-G. Chen, D. Liu, C.-C. Wu, Z.-X. Huang, T.-C. Lin, C.-H. Wu, M. Zhu, E. Y. Li, W.-Y. Hung, W. Zhu and P.-T. Chou, *Nat. Photonics*, 2021, **15**(10), 780.
32 D. Hall, K. Stavrou, E. Duda, A. Danos, S. Bagnich, S. Warriner, A. M. Z. Slawin, D. Beljonne, A. Kohler and A. Monkman, *et al.*, *Mater. Horiz.*, 2022, **9**(3), 1068.
33 C. Cao, J. H. Tan, Z. L. Zhu, J. D. Lin, H. J. Tan, H. Chen, Y. Yuan, M. K. Tse, W. C. Chen and C. S. Lee, *Angew. Chem., Int. Ed.*, 2023, **62**(10), e202215226.
34 X. F. Luo, F. L. Li, J. W. Zou, Q. Zou, J. Su, M. X. Mao and Y. X. Zheng, *Adv. Opt. Mater.*, 2021, **9**(21), 2100784.
35 W. H. Melhuish, *J. Phys. Chem.*, 1961, **65**(2), 229.
36 R. J. Holmes, S. R. Forrest, Y.-J. Tung, R. C. Kwong, J. J. Brown, S. Graon and M. E. Thompson, *Appl. Phys. Lett.*, 2003, **82**(15), 2422.
37 K. Zhang, J. Liu, Y. Zhang, J. Fan, C.-K. Wang and L. Lin, *J. Phys. Chem. C*, 2019, **123**(40), 24705.
38 Y.-Z. Shi, K. Wang, X.-C. Fan, H. Wu, X.-M. Ou, J. Yu, J.-S. Jie and X.-H. Zhang, *J. Mater. Chem. C*, 2022, **10**(12), 4717.
39 V. V. Pavlishchuk and A. W. Addison, *Inorg. Chim. Acta*, 2000, **298**(1), 97.
40 B. Dandrade, S. Datta, S. Forrest, P. Djurovich, E. Polikarpov and M. Thompson, *Org. Electron.*, 2005, **6**(1), 11.
41 (*a*) M. Fatahi, A. P. McKay, D. B. Cordes and E. Zysman-Colman, CCDC 2465301: Experimental Crystal Structure Determination, 2025, DOI: **10.5517/ccdc.csd.cc2nrbvm**; (*b*) M. Fatahi, A. P. McKay, D. B. Cordes and E. Zysman-Colman, CCDC 2465303: Experimental Crystal Structure Determination, 2025, DOI: **10.5517/ccdc.csd.cc2nrbxp**; (*c*) M. Fatahi, A. P. McKay, D. B. Cordes and E. Zysman-Colman, CCDC 2465304: Experimental Crystal Structure Determination, 2025, DOI: **10.5517/ccdc.csd.cc2nrbxp**.